Inorganic Chemistry

pubs.acs.org/IC Article

Large Manipulation of Ferrimagnetic Curie Temperature by A-Site Chemical Substitution in $ACu_3Fe_2Re_2O_{12}$ (A = Na, Ca, and La) Half Metals

Jie Zhang, Fedor Temnikov, Xubin Ye, Xiao Wang, Zhao Pan, Zhehong Liu, Maocai Pi, Shuai Tang, Chien-Te Chen, Chih-Wen Pao, Wei-Hsiang Huang, Chang-Yang Kuo, Zhiwei Hu, Yao Shen, Sergey V. Streltsov, and Youwen Long*

Cite This: *Inorg. Chem.* 2025, 64, 472−478

Read Online

ACCESS | Metrics & More | Article Recommendations

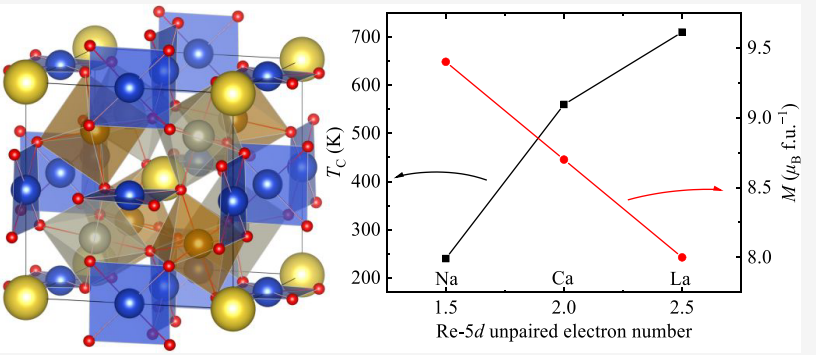

ABSTRACT: $CaCu_3Fe_2Re_2O_{12}$ and $LaCu_3Fe_2Re_2O_{12}$ quadruple perovskite oxides are well known for their high ferrimagnetic Curie temperatures and half-metallic electronic structures. By A-site chemical substitution with lower valence state Na^+, an isostructural compound $NaCu_3Fe_2Re_2O_{12}$ with both A- and B-site ordered quadruple perovskite structures in *Pn*−3 symmetry was prepared using high-pressure and high-temperature techniques. The X-ray absorption study demonstrates the valence states to be Cu^{2+}, Fe^{3+}, and $Re^{5.5+}$. A ferrimagnetic phase transition is found to take place at the Curie temperature $T_C \approx 240$ K, which is much less than that observed in A = Ca (560 K) and La (710 K) analogues. $NaCu_3Fe_2Re_2O_{12}$ possesses a larger saturated magnetic moment up to 9.4 μ_B/f.u. as well as a remarkably reduced coercive field less than 10 Oe at 2 K. Theoretical calculations suggest that $NaCu_3Fe_2Re_2O_{12}$ displays a half-metallic electronic band structure with complete spin polarization of conduction electrons in the minority-spin bands. The magnetic properties and electronic structures of the $ACu_3Fe_2Re_2O_{12}$ family are compared and discussed.

1. INTRODUCTION

ABO_3 perovskite oxides have been widely studied for their broadly diverse physical properties such as multiferroic property, negative thermal expansion, colossal magnetoresistance, and superconductivity.[1−10] In ABO_3, the A-site ions are typically rare earth, alkali, or alkaline earth metals with relatively large ionic radii, which form an AO_{12} tetradecahedral coordination environment, while B-site ions are transition metals that form BO_6 octahedral units connecting with each other by corner-sharing O atoms.[11] When three-quarters of the A-site ions are substituted by Jahn−Teller active magnetic ions like Mn^{3+} or Cu^{2+}, an A-site ordered quadruple perovskite oxide with the chemical formula of $AA'_3B_4O_{12}$ may be obtained.[12,13] Due to the relatively small ionic radii of A′-site ions (Mn^{3+} or Cu^{2+}), the $A'O_4$ square-coordinated units are prone to forming and connecting with BO_6 octahedra through corner-sharing of the O, resulting in an A′−O−B bond angle of about 110°. Concurrently, the BO_6 octahedra are inclined to heavily tilt, leading to a B−O−B bond angle of around 140°. Owing to the capability of incorporating transition metal cations at both A′ and B sites, $AA'_3B_4O_{12}$ quadruple perovskite oxides showcase intriguing electrical and magnetic characteristics. For example, $CaCu_3Ti_4O_{12}$ exhibits a weak temperature-dependent and high dielectric constant,[14,15] $LaCu_3Fe_4O_{12}$ displays intermetallic charge transfer and negative thermal expansion,[16] and multiferroic properties are found to occur in

Received: November 20, 2024
Revised: December 15, 2024
Accepted: December 19, 2024
Published: January 2, 2025

https://doi.org/10.1021/acs.inorgchem.4c04962
Inorg. Chem. 2025, 64, 472−478

$RMn_3Cr_4O_{12}$ (R = rare earth element or Bi),[17−20] $CaMn_3Mn_4O_{12}$,[21] and $CaFe_3Ti_4O_{12}$.[22]

Furthermore, for A-site ordered perovskite $AA'_3B_4O_{12}$, if B sites are occupied by two transition metals with large differences in ionic radius and/or valence states, an $AA'_3B_2B'_2O_{12}$-type both A- and B-site ordered quadruple perovskite is possible to obtain in a rock-salt ordered manner at B/B′ sites.[11] Thanks to the complex spin interactions among multiple atomic positions (A′, B, and B′ sites), fascinating physical properties are observed in $AA'_3B_2B'_2O_{12}$. For example, high-temperature ferrimagnetic ordering and variable electrical properties were reported in $ACu_3Fe_2Os_2O_{12}$ (A = Na, Ca, and La).[23−25] Specifically, in $CaCu_3Fe_2Os_2O_{12}$, a high Curie temperature T_C = 580 K and an energy band gap about 1.0 eV at room temperature were observed.[24] However, when Ca^{2+} is replaced by Na^+, the value of the Os^{5+} ($5d^3$) changes to that of the $Os^{5.5+}$ ($5d^{2.5}$), causing the electrical properties to change from insulating for A = Ca to metallic for A = Na. Moreover, the reduced number of unpaired electrons in Os weakens the magnetic coupling intensity of Fe−O−Os and Cu−O−Os pathways, leading to the decrease in the T_C from 580 K for A = Ca to 380 K for A = Na.[23] On the other hand, when Ca^{2+} is substituted by La^{3+} with a higher valence state, the average valence state of Os will decrease to +4.5, yielding the mixture of Os^{4+} ($5d^4$) and Os^{5+} ($5d^3$) in $LaCu_3Fe_2Os_2O_{12}$, which retains the insulation.[25] However, the presence of nonmagnetic Os^{4+} results in a slightly lower T_C in $LaCu_3Fe_2Os_2O_{12}$ (520 K) compared to that of $CaCu_3Fe_2Os_2O_{12}$.[24] Therefore, A-site ion substitution can exert a significant influence in manipulating the magnetic properties and electronic structures of $AA'_3B_2B'_2O_{12}$ quadruple perovskite oxides.

Compared with $ACu_3Fe_2Os_2O_{12}$ mentioned above, the $ACu_3Fe_2Re_2O_{12}$ family exhibits almost comparable Curie temperatures even though Re has fewer 5d electrons than does Os. For example, the T_C value of $CaCu_3Fe_2Re_2O_{12}$ is reported to be 560 K.[26] Moreover, this compound shows a half-metallic electronic structure with an energy gap in the majority-spin band.[26] By replacing Ca^{2+} with a higher valence state La^{3+}, the average valence state of Re is reduced from +5 to +4.5 in $LaCu_3Fe_2Re_2O_{12}$.[27] The presence of more unpaired 5d electrons in $Re^{4.5+}$ ($5d^{2.5}$) induces stronger magnetic interactions. Consequently, the T_C of $LaCu_3Fe_2Re_2O_{12}$ sharply rises to 710 K, while the half-metallic band structure remains unchanged, making $LaCu_3Fe_2Re_2O_{12}$ a promising half metal with the record high T_C in perovskite oxides.[27] It could be interesting to study the effect of low-valence state substitution at the A-site on the electronic structure and physical properties for the $ACu_3Fe_2Re_2O_{12}$ family. In this work, we succeeded in synthesizing both A- and B-site ordered quadruple perovskite $NaCu_3Fe_2Re_2O_{12}$ (NCFRO) for the first time. As expected, a hole is doped into the Re site in the presence of charge states of $Na^+/Cu^{2+}/Fe^{3+}/Re^{5.5+}$. Detailed magnetic and electrical properties were studied for NCFRO.

2. EXPERIMENTAL AND CALCULATION SECTION

The bulk polycrystalline NCFRO was synthesized using highly pure (>99.9%) NaOH, Fe_2O_3, CuO, Re, and Re_2O_7 powders as starting components. These reactants were well mixed with a stoichiometric ratio of 14:14:42:6:11 and sealed into a gold capsule after grinding thoroughly in an agate mortar. Then, the capsule was treated on a cubic anvil-type high-pressure apparatus at the settings of 9 GPa and 1273 K for half an hour. Once the heating period was completed, the pressure was gradually released back to ambient conditions over several hours. Finally, the obtained sample was dried at 400 K for 30 min to remove the possible residual water (H_2O) after the reaction of NaOH. The powder synchrotron X-ray diffraction (SXRD) data were collected at room temperature (RT) on beamline BL02B2 of SPring-8 in Japan with a λ = 0.70026 Å wavelength. The Rietveld refinement of SXRD data was performed using the GSAS program.[28] The X-ray absorption spectroscopy (XAS) measurements at the Cu/Fe-$L_{2,3}$ edges were carried out at beamline TLS11A with the total electron yield mode, and the Re-L_3 edge was recorded at TPS44A with the transmission mode in the National Synchrotron Radiation Research Center (NSRRC) of Taiwan at RT. The magnetic susceptibility was measured on a magnetic property measurement system (MPMS-VSM, Quantum Design) with field-cooled (FC) and zero-field-cooled (ZFC) modes with a field of 0.1 T in 2−390 K. Isothermal magnetization was measured at 2, 200, and 300 K, respectively. The electrical resistivity was measured from 2 to 320 K at 0 T field, and from −8 to 8 T at 2, 200, and 300 K, and specific heat measurement from 2 to 290 K at 0 T was performed on the physical property measurement system (PPMS-9 T, Quantum Design).

The spin-polarized electronic structure theoretical calculations were carried out by density functional theory (DFT) in the VASP code[29] using the generalized gradient approximation (GGA) method.[30] The crystallographic structures used in calculations were obtained from the SXRD refinement. Strong Coulomb correlations are taken into account via the GGA + U approach.[31] The effective Coulomb interactions $U_{eff} = U - J_H$ for Cu, Fe, and Re ions are 7.0, 4.1, and 2.5 eV, respectively, which are close to parameters used in literature.[32−34] The plane-wave energy cutoff is 520 eV, and k-mesh is 4 × 4 × 4. The convergence criterion for the total energy is 10^{-6} eV.

3. RESULTS AND DISCUSSION

Figure 1 depicts the SXRD data and the Rietveld refinement results of NCFRO at RT. The diffraction pattern can be refined well based on both A- and B-site ordered $AA'_3B_2B'_2O_{12}$-type quadruple perovskite structure model with the space group $Pn-3$. To evaluate the B-site degree of chemical order, the occupancy factors for A-site Na and A′-site Cu are fixed to unity owing to the large difference in ionic size between them. In addition, considering the nearly stoichiometric oxygen content (shown later), the occupancy factor of O is constrained to unity, too. Then, the ordering degree

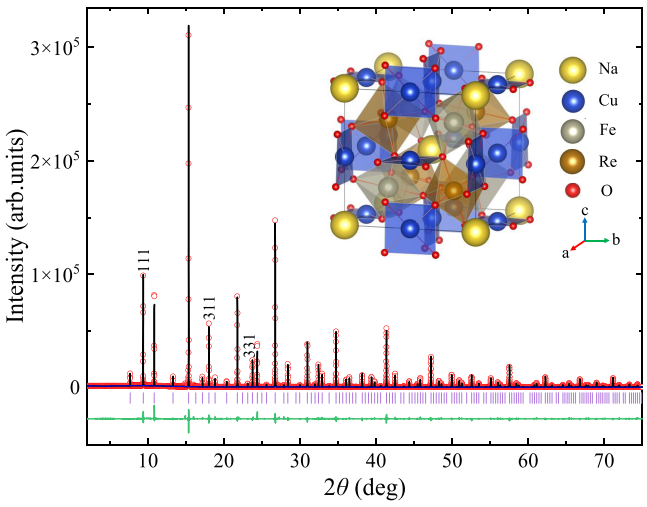

Figure 1. Pattern of SXRD data and Rietveld refinement results for NCFRO at RT. The experimental (red circles), simulated (black line), background (blue line), and difference (olive line at the bottom) patterns are displayed. The Bragg reflection positions for space group $Pn-3$ are displayed as purple ticks. The inset illustrates the schematic representation of the crystal structure for NCFRO.

https://doi.org/10.1021/acs.inorgchem.4c04962
Inorg. Chem. 2025, 64, 472−478

Table 1. Refined Structure Parameters of NCFRO at RT from SXRD Data[a]

site	WP	x	y	z	G	U_{iso} (100 × Å^2)
Na	2a	0.25	0.25	0.25	1.0	1.58(5)
Cu	6d	0.25	0.75	0.75	1.0	0.21(4)
Fe1	4b	0	0	0	0.980(1)	0.44(4)
Re1	4b	0	0	0	0.020(1)	0.44(4)
Re2	4c	0.5	0.5	0.5	0.980(1)	0.61(3)
Fe2	4c	0.5	0.5	0.5	0.020(1)	0.61(3)
O	24h	0.5664(5)	0.7562(4)	0.0576(4)	1.0	1.04(13)

bond length	value (Å)	bond angle	value (°)
Cu−O (×4)	1.974(3)	∠Fe1−O−Re2	141.3(2)
Fe1−O (×6)	2.010(3)	∠Cu−O−Fe1	107.5(1)
Re2−O (×6)	1.923(3)	∠Cu−O−Re2	111.1(2)
BVS (Cu)	2.07	BVS (Fe)	3.04

[a]Crystal data: space group $Pn\bar{3}$ (No. 201), a = 7.41960(1) Å. WP: Wyckoff position; G: site occupancy. R_{wp} = 8.41%, R_p = 6.03%. The formula $V_i = \sum_j S_{ij}$, and $S_{ij} = \exp[(r_0 - r_{ij})/0.37)]$ was used to calculate BVS values. The value of r_0 = 1.679 for Cu, 1.759 for Fe.

between the B-site Fe and B′-site Re is refined to be a high level of about 98.0%. Table 1 provides the refined structure parameters of NCFRO. Four of the Cu−O bonds are relatively short, signifying the formation of the fourfold square-planar coordination of CuO_4, as illustrated in the inset of Figure 1. The Fe/ReO_6 octahedra, which are linked with each other through corner-sharing of the atoms of O in a rock-salt-type ordered manner, connect with CuO_4 units by sharing of the O atoms. Based on the refined Cu−O and Fe−O bond lengths and the bond valence sum (BVS) calculations,[35] the valence states of Cu and Fe ions were suggested to be Cu^{2+} and Fe^{3+} (see Table 1). Meanwhile, NCFRO has the shortest Re−O bond length (1.923 Å) compared with that of the Fe/Re ordered perovskite oxides $CaCu_3Fe_2Re_2^{5+}O_{12}$ (1.934 Å),[26] $LaCu_3Fe_2Re_2^{4.5+}O_{12}$ (1.960 Å),[27] $Ca_2FeRe^{5+}O_6$ (1.951 Å in average), and $Sr_2FeRe^{5+}O_6$ (1.956 Å in average),[36,37] implying the presence of a higher charge state of Re in NCFRO as confirmed by the XAS measurement results described subsequently.

To validate the valence configuration of NCFRO, we performed XAS measurement, which is well known due to its element selectivity and sensitivity for the valence states as well as the local environment of transition metals.[38] As displayed in Figure 2a,b, the white line of Cu-$L_{2,3}$ (Fe-$L_{2,3}$) exhibits similar characteristics with the peak energies as the reference compound $CaCu_3^{2+}Ti_4O_{12}$[39] ($LaCu_3Fe_2^{3+}Re_2O_{12}$[27]), indicating the existence of the Cu^{2+} (Fe^{3+}) valence state. As shown in Figure 2c, the peak of Re-L_3 XAS in NCFRO is located at an intermediate position between those of $Sr_2MgRe^{6+}O_6$[40] and $Sr_2FeRe^{5+}O_6$,[41] suggesting the formation of a $Re^{5.5+}$ state. Therefore, the charge configuration of NCFRO is assigned to be $Na^+Cu_3^{2+}Fe_2^{3+}Re_2^{5.5+}O_{12}$, which also reveals the stoichiometric chemical composition for this compound. In comparison, the charge states of Cu and Fe remain unchanged in $CaCu_3Fe_2Re_2O_{12}$ and the current NCFRO. However, a hole was doped into the Re site in NCFRO by substituting Ca^{2+} at the A-site with low-valence state Na^+.

Figure 3a displays the temperature dependence of the magnetic susceptibility of NCFRO. As the temperature decreases, the ZFC and FC curves sharply rise at $T_C \approx 240$ K (determined by a tangent method), suggesting a ferro- or ferrimagnetic phase transition. As displayed in Figure 3b, above T_C, the isothermal magnetization curve of NCFRO has a nearly linear behavior, agreeing with the paramagnetic state.

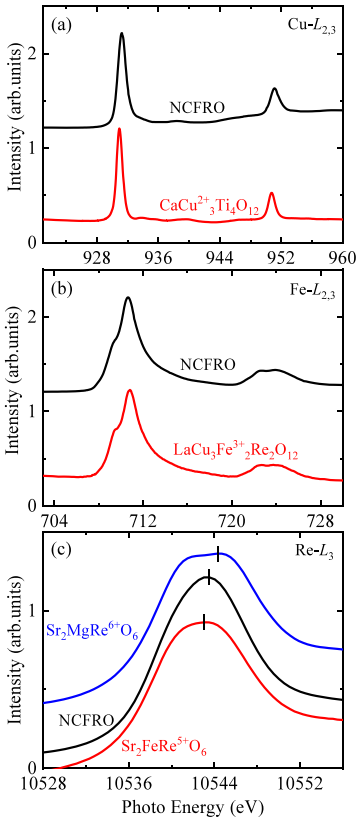

Figure 2. XAS spectra of (a) Cu-$L_{2,3}$ edges together with that of Cu^{2+} reference $CaCu_3T_{i4}O_{12}$, (b) Fe-$L_{2,3}$ edges together with that of Fe^{3+} reference $LaCu_3Fe_2^{3+}Re_2O_{12}$, and (c) Re-$L_3$ edge with Re^{6+} of Sr_2MgReO_6 and Re^{5+} of Sr_2FeReO_6 for NCFRO.

However, the magnetization exhibits typical magnetic hysteresis at temperatures below T_C, which further indicates the ferro- or ferrimagnetic nature of NCFRO. Meanwhile, one finds that the saturated magnetic moment increases with decreasing temperature and reaches 9.4 μ_B/f.u. at 2 K and 7 T, which is close to the theoretical spin-only value (10.0 μ_B/f.u.) obtained by considering a colinear ferrimagnetic arrangement of $Cu^{2+}(\uparrow)-Fe^{3+}(\uparrow)-Re^{5.5+}(\downarrow)$. As is well known that the isostructural compounds Ca/$LaCu_3Fe_2Re_2O_{12}$ possess the magnetic configuration of $Cu(\uparrow)-Fe(\uparrow)-Re(\downarrow)$,[26,27] a similar ferrimagnetic alignment is expected to occur in the current NCFRO. Therefore, a ferrimagnetic phase transition with the

https://doi.org/10.1021/acs.inorgchem.4c04962
Inorg. Chem. 2025, 64, 472−478

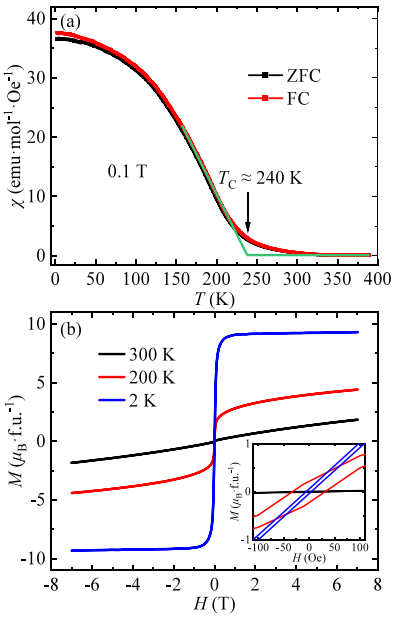

Figure 3. (a) Temperature-dependent magnetic susceptibility with ZFC and FC modes under the 0.1 T field for NCFRO. The green lines are tangents to determine the T_C. (b) Magnetic field dependence of magnetization recorded at three selected temperatures for NCFRO. The inset demonstrates an enlarged view of the low field range.

$Cu^{2+}(\uparrow)-Fe^{3+}(\uparrow)-Re^{5.5+}(\downarrow)$ spin coupling is rationally assigned for NCFRO at $T_C \approx 240$ K. Moreover, the coercive field of NCFRO is extremely small with the value of only about 40 Oe at 200 K and decreases to below 10 Oe at 2 K, as shown in the inset of Figure 3b, demonstrating the exceptional soft magnetic property for NCFRO. In comparison, the coercive field observed in $Ca/LaCu_3Fe_2Re_2O_{12}$ is about 100 Oe at 2 K.[26,27]

The temperature-dependent electrical resistivity for NCFRO is shown in Figure 4. It exhibits an order of 1 mΩ·cm among

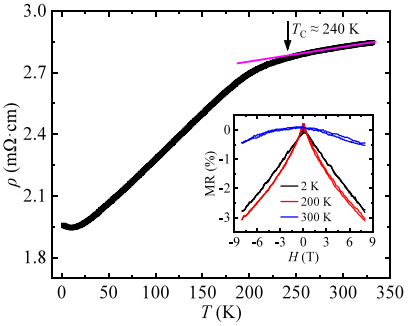

Figure 4. Temperature dependence of electrical resistivity for NCFRO from 2 to 320 K measured at zero field. The pink line represents a linear fit in the region above T_C. The inset depicts the MR [MR = 100% × [ρ (H) − ρ (0 T))/ρ (0 T)] effects measured at 2, 200, and 300 K, respectively.

the whole temperature range we measured and decreases continuously as the temperature decreases, indicating a metal-like transport behavior for this compound. Above T_C, the resistivity seems to decline slowly and linearly with decreasing temperature. Below T_C, the rate of resistivity change becomes more pronounced, probably due to the weakening of carrier scattering caused by thermally agitated spins for the ferrimagnetic state.[42] The upturn below 15 K could be attributed to the grain boundary effects of the polycrystalline sample.[26] The inset of Figure 4 depicts the magnetoresistance (MR) effect [MR = 100% × (ρ (H) − ρ (0 T))/ρ (0 T)] of NCFRO as the function of the magnetic field at 2, 200, and 300 K. At 300 K, NCFRO exhibits a very weak negative MR effect, suggesting that the carrier scattering due to disordered spins is barely affected by the magnetic field at temperatures above T_C. Below T_C, the negative MR features are relatively pronounced with the absolute value of MR increasing as the field increases, mainly because magnetic fields can suppress spin fluctuations and uniformly align magnetic domains that reduces the carrier scattering.[43,44]

Figure 5 displays the specific heat as a dependence of temperature for NCFRO. No obvious anomaly is found to

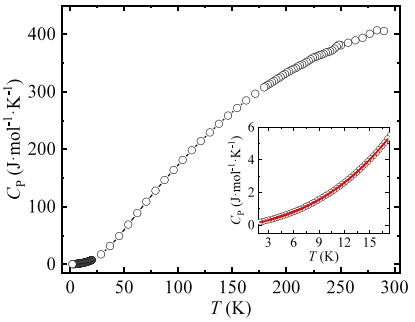

Figure 5. Specific heat data as a dependence of temperature for NCFRO from 2 to 290 K measured at 0 T field. The inset displays the fitting result (red line) based on the function $C_p = \gamma T + \beta T^3 + \alpha T^{3/2}$ from 2 to 18 K.

occur throughout the measurement temperature range in 2−290 K. The absence of a distinct phase transition peak around T_C in specific heat may be due to the slow establishment of ferrimagnetic ordering, leading to a gradual release of magnetic entropy in a wide temperature window. A similar phenomenon was also reported in another isostructural compound $LaCu_3Co_2Re_2O_{12}$.[45] As depicted in the inset of Figure 5, the low-temperature (2−18 K) specific heat data of NCFRO can be well described by the function $C_p = \gamma T + \beta T^3 + \alpha T^{3/2}$, in which the T term stands for the contribution of delocalized electrons, the T^3 term represents the phonons and antiferromagnetic contribution, and the $T^{3/2}$ term originates from the ferromagnetic excitation contribution. The coefficients were fitted to be γ = 44.4(9) mJ·mol^{-1}·K^{-2}, α = 30.3(4) mJ·mol^{-1}·K$^{-5/2}$, and β = 0.46(3) mJ·mol^{-1}·K^{-4}. The considerable value of the Sommerfeld coefficient γ suggests a remarkable electronic contribution to specific heat, which provides additional support for the intrinsic metal-like nature of NCFRO.

Spin-polarized electronic structure calculations utilizing the DFT with the electronic correlation effect (U) were conducted to further analyze the electronic properties of NCFRO. The theoretically calculated band structures and the density of states (DOS) are shown in Figure 6. An energy gap of approximately 2.0 eV in the majority (up)-spin bands is observed. However, the Fermi level crosses the minority (down)-spin bands primarily composed of Re 5d states hybridized with the state of O 2p and a few Cu 3d and Fe 3d states. Therefore, the NCFRO exhibits a half-metallic ground state with fully polarized minority (down)-spin conduction electrons. Furthermore, the 3d orbital electrons

https://doi.org/10.1021/acs.inorgchem.4c04962
Inorg. Chem. 2025, 64, 472−478

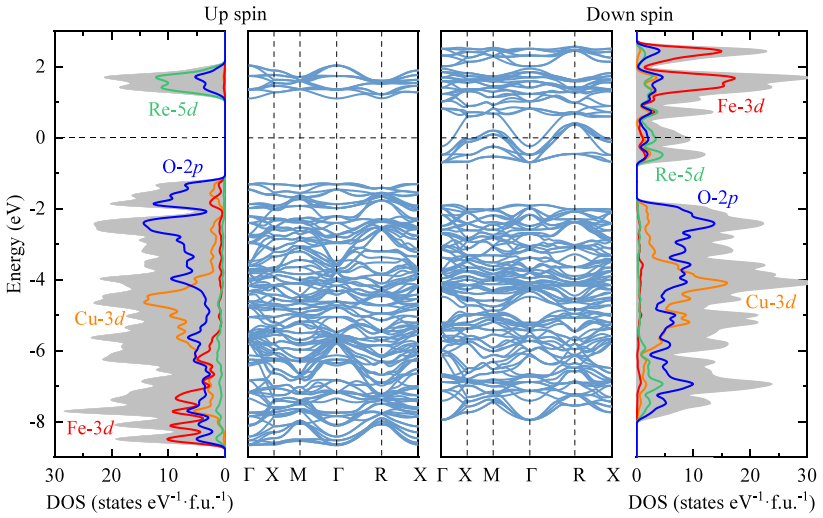

Figure 6. Calculated spin-polarized band structures and the DOS near the Fermi level (set to zero) of NCFRO using the GGA + U method with U_{eff} = 7 eV for Cu, 4.1 eV for Fe, and 2.5 eV for Re, respectively. The total DOS (ashen shadow) and individual DOS of Cu 3d (orange line), Fe 3d (red line), Re 5d (green line), and O 2p (blue line) are displayed.

of Fe^{3+} predominantly occupy the up-spin bands, and Cu^{2+} 3d up-spin bands are almost fully filled, while the 5d electrons of the $Re^{5.5+}$ are primarily found in the down-spin bands. This configuration aligns with the Cu(↑)−Fe(↑)−Re(↓) ferrimagnetic arrangement discussed previously.

In the $ACu_3Fe_2Re_2O_{12}$ (A = Na, Ca, and La) family, all the members display half-metallic electronic structures with an energy band gap in the majority (up)-spin bands, and predominant Re 5d orbitals, where t_{2g} orbitals always have fewer than half the electrons regardless of the valence state of the A-site ion, hybridized with O 2p and a few Cu/Fe 3d orbitals compose the partially filled down-spin bands around the Fermi level. As depicted by the schematic DOS including Cu, Fe, and Re bands for $ACu_3Fe_2Re_2O_{12}$ in Figure 7a, when

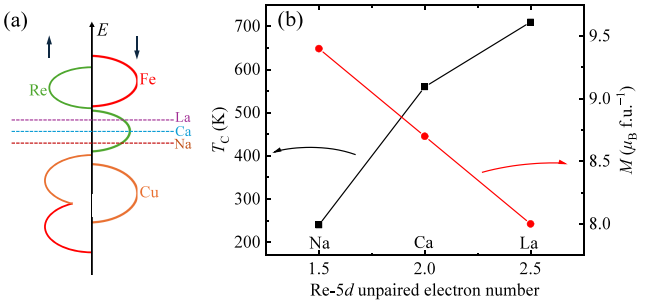

Figure 7. (a) Schematic DOS of Cu (orange), Fe (red), and Re (green) around the Fermi level of $ACu_3Fe_2Re_2O_{12}$. The dashed lines represent the Fermi level. (b) Re 5d unpaired electron number dependence of T_C and saturated magnetization measured at 2 K for the $ACu_3Fe_2Re_2O_{12}$ family.

the A-site ions change from La^{3+} to Na^+, the hole doping causes the Fermi level to move downward without significantly altering the DOS shape, due to the robust cubic quadruple perovskite structure, and therefore the electron number of Re 5d down-spin orbitals is reduced. Moreover, the A-site chemical substitution with different valence states has a significant influence on the T_C value for $ACu_3Fe_2Re_2O_{12}$. The T_C for A = La (710 K) is higher than that of A = Ca (560 K), and the T_C of A = Na (240 K) is much lower.[26,27] As shown in Figure 7b, the fewer the unpaired electrons of Re 5d orbitals from A = La to Ca, and to Na, the lower the T_C. Therefore, the weakness of exchange interaction is mainly attributed to the decreased number of unpaired electrons in 5d orbitals of Re ions, which decreases the dominant Cu−Re and Fe−Re magnetic coupling,[26,27,46] leading to a lower T_C. On the other hand, the saturated moment at 2 K increases as the number of electrons of Re ions decreases, as displayed in Figure 7b. This is because the moment of Re ions, which are antiparallel to those of Cu and Fe, has a smaller counteracting effect on the total magnetic moments from A = La to Na, resulting in the largest saturated magnetization in the NCFRO.

4. CONCLUSIONS

In summary, we synthesized a new A- and B-site ordered quadruple perovskite oxide, $NaCu_3Fe_2Re_2O_{12}$, with the $Pn-3$ space group and a charge combination of $Na^+/Cu^{2+}/Fe^{3+}/Re^{5.5+}$ using high-pressure and high-temperature methods. This material is a ferrimagnet with a T_C of about 240 K. A large saturated moment of 9.4 μ_B/f.u. and a small magnetic coercive field of less than 10 Oe at 2 K were observed. Theoretical calculations suggest that $NaCu_3Fe_2Re_2O_{12}$ has a half-metallic electronic structure with completely spin-polarized conduction electrons in the minority-spin bands. By comparing with Ca/$LaCu_3Fe_2Re_2O_{12}$, we conclude that the low-valence ion substitution of the A site can significantly reduce T_C due to reduced antiferromagnetic interactions for Cu−Re and Fe−Re from the decreased number of unpaired 5d electrons in Re ions.

AUTHOR INFORMATION

Corresponding Author

Youwen Long − *Beijing National Laboratory for Condensed Matter Physics, Institute of Physics, Chinese Academy of Sciences, Beijing 100190, China; School of Physical Sciences, University of Chinese Academy of Sciences, Beijing 100049, China; Songshan Lake Materials Laboratory, Dongguan, Guangdong 523808, China;* orcid.org/0000-0002-8587-7818; Email: ywlong@iphy.ac.cn

https://doi.org/10.1021/acs.inorgchem.4c04962
Inorg. Chem. 2025, 64, 472−478

Authors

Jie Zhang − *Beijing National Laboratory for Condensed Matter Physics, Institute of Physics, Chinese Academy of Sciences, Beijing 100190, China; School of Physical Sciences, University of Chinese Academy of Sciences, Beijing 100049, China;* orcid.org/0009-0006-9055-2969

Fedor Temnikov − *Institute of Metal Physics, Ekaterinburg 620108, Russia*

Xubin Ye − *Beijing National Laboratory for Condensed Matter Physics, Institute of Physics, Chinese Academy of Sciences, Beijing 100190, China;* orcid.org/0000-0002-5739-8318

Xiao Wang − *Beijing National Laboratory for Condensed Matter Physics, Institute of Physics, Chinese Academy of Sciences, Beijing 100190, China;* orcid.org/0000-0001-8139-4192

Zhao Pan − *Beijing National Laboratory for Condensed Matter Physics, Institute of Physics, Chinese Academy of Sciences, Beijing 100190, China;* orcid.org/0000-0002-8693-2508

Zhehong Liu − *Beijing National Laboratory for Condensed Matter Physics, Institute of Physics, Chinese Academy of Sciences, Beijing 100190, China*

Maocai Pi − *Beijing National Laboratory for Condensed Matter Physics, Institute of Physics, Chinese Academy of Sciences, Beijing 100190, China; School of Physical Sciences, University of Chinese Academy of Sciences, Beijing 100049, China*

Shuai Tang − *Beijing National Laboratory for Condensed Matter Physics, Institute of Physics, Chinese Academy of Sciences, Beijing 100190, China;* orcid.org/0009-0008-5092-067X

Chien-Te Chen − *National Synchrotron Radiation Research Center, Hsinchu 30076, Taiwan*

Chih-Wen Pao − *National Synchrotron Radiation Research Center, Hsinchu 30076, Taiwan;* orcid.org/0000-0001-7681-4391

Wei-Hsiang Huang − *National Synchrotron Radiation Research Center, Hsinchu 30076, Taiwan*

Chang-Yang Kuo − *National Synchrotron Radiation Research Center, Hsinchu 30076, Taiwan; Department of Electrophysics, National Yang Ming Chiao Tung University, Hsinchu 30010, Taiwan*

Zhiwei Hu − *Max Planck Institute for Chemical Physics of Solids, Dresden 01187, Germany;* orcid.org/0000-0003-0324-2227

Yao Shen − *Beijing National Laboratory for Condensed Matter Physics, Institute of Physics, Chinese Academy of Sciences, Beijing 100190, China; School of Physical Sciences, University of Chinese Academy of Sciences, Beijing 100049, China*

Sergey V. Streltsov − *Institute of Metal Physics, Ekaterinburg 620108, Russia; Department of Theoretical Physics and Applied Mathematics, Ural Federal University, Ekaterinburg 620002, Russia*

Complete contact information is available at: https://pubs.acs.org/10.1021/acs.inorgchem.4c04962

Notes

The authors declare no competing financial interest.

■ ACKNOWLEDGMENTS

This work was supported by the National Key R&D Program of China (Grant No. 2021YFA1400300), the National Natural Science Foundation of China (Grant Nos. 12261131499, 12425403, 11934017, 11921004, 22271309, 12204516, 12304159, and 12304268), the Chinese Academy of Sciences (Grant No. XDB33000000), and the China Postdoctoral Science Foundation (Grant No. 2023M743741). Theoretical DFT calculations were supported by the "Quantum" project (122021000038-7). Treatment of correlation effects by the DFT + U approach was supported by the Russian Science Foundation (grant RSF 23-42-00069). Dr. Zhiwei Hu acknowledges the support from the Max Planck-POSTECH-Hsinchu Center for Complex Phase Materials. The powder synchrotron X-ray diffraction experiments were performed at SPring-8 with the approval of the Japan Synchrotron Radiation Research Institute (2023B1575).

■ REFERENCES

(1) Kimura, T.; Goto, T.; Shintani, H.; Ishizaka, K.; Arima, T.; Tokura, Y. Magnetic control of ferroelectric polarization. *Nature* **2003**, *426*, 55.

(2) Wang, J.; Neaton, J. B.; Zheng, H.; Nagarajan, V.; Ogale, S. B.; Liu, B.; Viehland, D.; Vaithyanathan, V.; Schlom, D. G.; Waghmare, U. V.; Spaldin, N. A.; Rabe, K. M.; Wuttig, M.; Ramesh, R. Epitaxial $BiFeO_3$ multiferroic thin film heterostructures. *Science* **2003**, *299*, 1719.

(3) Choi, T.; Lee, S.; Choi, Y. J.; Kiryukhin, V.; Cheong, S.-W. Switchable ferroelectric diode and photovoltaic effect in $BiFeO_3$. *Science* **2009**, *324*, 63.

(4) Azuma, M.; Chen, W.-T.; Seki, H.; Czapski, M.; Olga, S.; Oka, K.; Mizumaki, M.; Watanuki, T.; Ishimatsu, N.; Kawamura, N.; Ishiwata, S.; Tucker, M. G.; Shimakawa, Y.; Attfield, J. P. Colossal negative thermal expansion in $BiNiO_3$ induced by intermetallic charge transfer. *Nat. Commun.* **2011**, *2*, 347.

(5) Pan, Z.; Chen, J.; Jiang, X.; Hu, L.; Yu, R.; Yamamoto, H.; Ogata, T.; Hattori, Y.; Guo, F.; Fan, X.; Li, G.; Gu, H.; Ren, Y.; Lin, Z.; Azuma, M.; Xing, X. Colossal volume contraction in strong polar perovskites of $Pb(Ti,V)O_3$. *J. Am. Chem. Soc.* **2017**, *139*, 14865.

(6) Coey, J. M. D.; Viret, M. V.; Von Molnar, S. Mixed-valence manganites. *Adv. Phys.* **1999**, *48*, 167.

(7) Tokura, Y. Critical features of colossal magnetoresistive manganites. *Rep. Prog. Phys.* **2006**, *69*, 797.

(8) Cava, R. J.; Batlogg, B.; Van Dover, R. B.; Murphy, D. W.; Sunshine, S.; Siegrist, T.; Remeika, J. P.; Rietman, E. A.; Zahurak, S.; Espinosa, G. P. Bulk superconductivity at 91 K in single-phase oxygen-deficient perovskite $Ba_2YCu_3O_{9-\delta}$. *Phys. Rev. Lett.* **1987**, *58*, 1676.

(9) Reyren, N.; Thiel, S.; Caviglia, A. D.; Kourkoutis, L. F.; Hammerl, G.; Richter, C.; Schneider, C. W.; Kopp, T.; Rüetschi, A.-S.; Jaccard, D.; Gabay, M.; Muller, D. A.; Triscone, J.-M.; Mannhart, J. Superconducting interfaces between insulating oxides. *Science* **2007**, *317*, 1196.

(10) Cohen, R. E. Origin of ferroelectricity in perovskite oxides. *Nature* **1992**, *358*, 136.

(11) King, G.; Woodward, P. M. Cation ordering in perovskites. *J. Mater. Chem.* **2010**, *20*, 5785.

(12) Bochu, B.; Chenavas, J.; Joubert, J. C.; Marezio, M. High pressure synthesis and crystal structure of a new series of perovskite-like compounds CMn_7O_{12} (C = Na, Ca, Cd, Sr, La, Nd). *J. Solid State Chem.* **1974**, *11*, 88.

(13) Chenavas, J.; Joubert, J. C.; Marezio, M.; Bochu, B. The synthesis and crystal structure of $CaCu_3Mn_4O_{12}$: A new ferromagnetic-perovskite-like compound. *J. Solid State Chem.* **1975**, *14*, 25.

(14) Ramirez, A. P.; Subramanian, M. A.; Gardel, M.; Blumberg, G.; Li, D.; Vogt, T.; Shapiro, S. M. Giant dielectric constant response in a copper-titanate. *Solid State Commun.* **2000**, *115*, 217.

(15) Zhu, Y.; Zheng, J. C.; Wu, L.; Frenkel, A. I.; Hanson, J.; Northrup, P.; Ku, W. Nanoscale disorder in $CaCu_3Ti_4O_{12}$: a new route to the enhanced dielectric response. *Phys. Rev. Lett.* **2007**, *99*, No. 037602.
(16) Long, Y.; Hayashi, N.; Saito, T.; Azuma, M.; Muranaka, S.; Shimakawa, Y. Temperature-induced A-B intersite charge transfer in an A-site-ordered $LaCu_3Fe_4O_{12}$ perovskite. *Nature* **2009**, *458*, 60.
(17) Wang, X.; Chai, Y.; Zhou, L.; Cao, H.; Cruz, C.-d.; Yang, J.; Dai, J.; Yin, Y.; Yuan, Z.; Zhang, S.; Yu, R.; Azuma, M.; Shimakawa, Y.; Zhang, H.; Dong, S.; Sun, Y.; Jin, C.; Long, Y. Observation of magnetoelectric multiferroicity in a cubic perovskite system: $LaMn_3Cr_4O_{12}$. *Phys. Rev. Lett.* **2015**, *115*, No. 087601.
(18) Liu, G.; Liu, Z.; Chai, Y.; Zhou, L.; Shen, X.; Ye, X.; Qin, S.; Lu, D.; Hu, Z.; Tjeng, L. H.; Lin, H.-J.; Chen, C.-T.; Yu, X.; Long, Y. Magnetic and electric field dependent anisotropic magnetoelectric multiferroicity in $SmMn_3Cr_4O_{12}$. *Phys. Rev. B* **2021**, *104*, No. 054407.
(19) Zhou, L.; Dai, J.; Chai, Y.; Zhang, H.; Dong, S.; Cao, H.; Calder, S.; Yin, Y.; Wang, X.; Shen, X.; Liu, Z.; Saito, T.; Shimakawa, Y.; Hojo, H.; Ikuhara, Y.; Azuma, M.; Hu, Z.; Sun, Y.; Jin, C.; Long, Y. Realization of large electric polarization and strong magnetoelectric coupling in $BiMn_3Cr_4O_{12}$. *Adv. Mater.* **2017**, *29*, No. 1703435.
(20) Liu, G.; Pi, M.; Zhou, L.; Liu, Z.; Shen, X.; Ye, X.; Qin, S.; Mi, X.; Chen, X.; Zhao, L.; Zhou, B.; Guo, J.; Yu, X.; Chai, Y.; Weng, H.; Long, Y. Physical realization of topological Roman surface by spin-induced ferroelectric polarization in cubic lattice. *Nat. Commun.* **2022**, *13*, 2373.
(21) Johnson, R. D.; Chapon, L. C.; Khalyavin, D. D.; Manuel, P.; Radaelli, P. G.; Martin, C. (2012) Giant improper ferroelectricity in the ferroaxial magnet $CaMn_7O_{12}$. *Phys. Rev. Lett.* **2012**, *108*, No. 067201.
(22) Lu, D.; Sheptyakov, D.; Cao, Y.; Zhao, H.; Zhang, J.; Pi, M.; Ye, X.; Liu, Z.; Zhang, X.; Pan, Z.; Jiang, X.; Hu, Z.; Yang, Y.-f; Yu, P.; Long, Y. Magnetic-field controllable displacement-type ferroelectricity driven by off-center Fe^{2+} Ions in $CaFe_3Ti_4O_{12}$ perovskite. *Adv. Funct. Mater.* **2024**, 2411133.
(23) Wang, X.; Liu, M.; Shen, X.; Liu, Z.; Hu, Z.; Chen, K.; Ohresser, P.; Nataf, L.; Baudelet, F.; Lin, H.-J.; Chen, C.-T.; Soo, Y.-L.; Yang, Y.-f.; Long, Y. High-temperature ferrimagnetic half metallicity with wide spin-up energy gap in $NaCu_3Fe_2Os_2O_{12}$. *Inorg. Chem.* **2018**, *58*, 320.
(24) Deng, H.; Liu, M.; Dai, J.; Hu, Z.; Kuo, C.; Yin, Y.; Yang, J.; Wang, X.; Zhao, Q.; Xu, Y.; Fu, Z.; Cai, J.; Guo, H.; Jin, K.; Pi, T.; Soo, Y.; Zhou, G.; Cheng, J.; Chen, K.; Ohresser, P.; Yang, Y.-f; Jin, C.; Tjeng, L.-H.; Long, Y. Strong enhancement of spin ordering by A-site magnetic ions in the ferrimagnet $CaCu_3Fe_2Os_2O_{12}$. *Phys. Rev. B* **2016**, *94*, No. 024414.
(25) Wang, X.; Liu, Z.; Ye, X.; Zhou, B.; Hu, Z.; Wang, W.; Yu, R.; Agrestini, S.; Zhou, G.; Chen, K.; Choueikani, F.; Ohresser, P.; Baudelet, F.; Lin, H.-J.; Chen, C.-T.; Tanaka, A.; Weng, S.-C.; Long, Y. Os doping suppressed Cu-Fe charge transfer and induced structural and magnetic phase transitions in $LaCu_3Fe_{4-x}Os_xO_{12}$ (x = 1 and 2). *Inorg. Chem.* **2021**, *60*, 6298.
(26) Chen, W.-t.; Mizumaki, M.; Seki, H.; Senn, M. S.; Saito, T.; Kan, D.; Attfield, J. P.; Shimakawa, Y. A half-metallic A- and B-site-ordered quadruple perovskite oxide $CaCu_3Fe_2Re_2O_{12}$ with large magnetization and a high transition temperature. *Nat. Commun.* **2014**, *5*, 3909.
(27) Liu, Z.; Zhang, S.; Wang, X.; Ye, X.; Qin, S.; Shen, X.; Lu, D.; Dai, J.; Cao, Y.; Chen, K.; Radu, F.; Wu, W. B.; Chen, C.-T.; Francoual, S.; Mardegan, J. R. L.; Leupold, O.; Tjeng, L. H.; Hu, Z.; Yang, Y.-f.; Long, Y. Realization of a half metal with a record-high Curie temperature in perovskite oxides. *Adv. Mater.* **2022**, *34*, No. 2200626.
(28) Rietveld, H. A profile refinement method for nuclear and magnetic structures. *J. Appl. Crystallogr.* **1969**, *2*, 65.
(29) Kresse, G.; Furthmüller, J. Efficient iterative schemes for Ab initio total-energy calculations using a plane-wave basis set. *Phys. Rev. B* **1996**, *54*, 11169.
(30) Perdew, J. P.; Burke, K.; Ernzerhof, M. Generalized gradient approximation made simple. *Phys. Rev. Lett.* **1996**, *77*, 3865.
(31) Dudarev, S. L.; Botton, G. A.; Savrasov, S. Y.; Humphreys, C. J.; Sutton, A. P. Electron-energy-loss spectra and the structural stability of nickel oxide: An LSDA + U study. *Phys. Rev. B* **1998**, *57*, 1505.
(32) Pchelkina, Z. V.; Komleva, E. V.; Irkhin, V. Yu.; Long, Y.; Streltsov, S. V. Rattling phonon modes in quadruple perovskites. *JETP Lett.* **2023**, *118*, 738.
(33) Pchelkina, Z. V.; Streltsov, S. V. Ab initio investigation of the exchange interactions in $Bi_2Fe_4O_9$: The Cairo pentagonal lattice compound. *Phys. Rev. B* **2013**, *88*, No. 054424.
(34) Merkel, M. E.; Tehrani, A. M.; Ederer, C. Probing the Mott insulating behavior of Ba_2MgReO_6 with DFT + DMFT. *Phys. Rev. Research* **2024**, *6*, No. 023233.
(35) Brown, I. D.; Altermatt, D. Bond-valence parameters obtained from a systematic analysis of the inorganic crystal structure database. *Acta Crystallogr.* **1985**, *41*, 244.
(36) Kato, H.; Okuda, T.; Okimoto, Y.; Tomioka, Y.; Oikawa, K.; Kamiyama, T.; Tokura, Y. Structural and electronic properties of the ordered double perovskites A_2MReO_6 (A = Sr, Ca; M = Mg, Sc, Cr, Mn, Fe, Co, Ni, Zn). *Phys. Rev. B* **2004**, *69*, No. 184412.
(37) Chen, J.; Feng, H. L.; Yamaura, K. Review of progress in the materials development of Re, Os, and Ir-based double perovskite oxides. *Mater. Today Phys.* **2024**, *40*, No. 101302.
(38) Burnus, T.; Hu, Z.; Wu, H.; Cezar, J. C.; Niitaka, S.; Takagi, H.; Chang, C. F.; Brookes, N. B.; Lin, H.-J.; Jang, L. Y.; Tanaka, A.; Liang, K. S.; Chen, C.-T.; Tjeng, L. H. X-ray absorption and x-ray magnetic dichroism study on Ca_3CoRhO_6 and Ca_3FeRhO_6. *Phys. Rev. B* **2008**, *77*, No. 205111.
(39) McGuinness, C.; Downes, J. E.; Sheridan, P.; Glans, P. A.; Smith, K. E.; Si, W.; Johnson, P. D. X-ray spectroscopic study of the electronic structure of the high-dielectric-constant material $CaCu_3Ti_4O_{12}$. *Phys. Rev. B* **2005**, *71*, No. 195111.
(40) Wiebe, C. R.; Greedan, J. E.; Kyriakou, P. P.; Luke, G. M.; Gardner, J. S.; Fukaya, A.; Gat-Malureanu, I. M.; Russo, P. L.; Savici, A. T.; Uemura, Y. J. Frustration-driven spin freezing in the S = 1/2 fcc perovskite Sr_2MgReO_6. *Phys. Rev. B* **2003**, *68*, No. 134410.
(41) Herrero-Martín, J.; Subías, G.; Blasco, J.; García, J.; Sánchez, M. C. X-ray absorption spectroscopic study on A_2FeReO_6 double perovskites. *J. Phys.: Condens. Matter* **2005**, *17*, 4963.
(42) Kato, H.; Okuda, T.; Okimoto, Y.; Tomioka, Y.; Takenoya, Y.; Ohkubo, A.; Kawasaki, M.; Tokura, Y. Metallic ordered double-perovskite Sr_2CrReO_6 with maximal Curie temperature of 635 K. *Appl. Phys. Lett.* **2002**, *81*, 328.
(43) Hwang, H. Y.; Cheong, S.-W.; Ong, N. P.; Batlogg, B. Spin-polarized intergrain tunneling in $La_{2/3}Sr_{1/3}MnO_3$. *Phys. Rev. Lett.* **1996**, *77*, 2041.
(44) Coey, J. M. D. Powder magnetoresistance (invited). *J. Appl. Phys.* **1999**, *85*, 5576.
(45) Liu, Z.; Sun, Q.; Ye, X.; Wang, X.; Zhou, L.; Shen, X.; Chen, K.; Nataf, L.; Baudelet, F.; Agrestini, S.; Chen, C.-T.; Lin, H.-J.; Vasili, H. B.; Valvidares, M.; Hu, Z.; Yang, Y.-f.; Long, Y. Quadruple perovskite oxide $LaCu_3Co_2Re_2O_{12}$: A ferrimagnetic half metal with nearly 100% B-site degree of order. *Appl. Phys. Lett.* **2020**, *117*, No. 152402.
(46) Wang, D.; Shaikh, M.; Ghosh, S.; Sanyal, B. Prediction of half-metallic ferrimagnetic quadruple perovskites $ACu_3Fe_2Re_2O_{12}$ (A = Ca, Sr, Ba, Pb, Sc, Y, La) with high Curie temperatures. *Phys. Rev. Mater.* **2021**, *5*, No. 054405.

https://doi.org/10.1021/acs.inorgchem.4c04962
Inorg. Chem. 2025, 64, 472−478